INTERNATIONAL JOURNAL FOR NUMERICAL METHODS IN FLUIDS, VOL. 6, 769–787 (1986)

TURBULENT BOUNDARY-LAYER ANALYSIS USING FINITE ELEMENTS

M. SHARMA AND G. F. CAREY

Department of Aerospace Engineering and Engineering Mechanics, The University of Texas at Austin, Austin, TX 78712, U.S.A.

SUMMARY

The use of finite element methods for turbulent boundary-layer flow is relatively recent and of limited extent.[1] In the present study, we extend the group variable approach of Fletcher and Fleet[2,3] to treat turbulent boundary layer flows with heat transfer using a two-equation turbulence model. The main concepts in the formulations include a Dorodnitsyn-type transformation which uses a velocity component as the transverse variable, a 'variational' formulation for the transformed equations using special test functions and development of a two-equation turbulence model in terms of the turbulent kinetic energy and turbulence dissipation rate as additional field variables. Several numerical test cases have been examined comparing the results with finite difference calculations and comparing the two-equation turbulence model with an algebraic turbulence model.

KEY WORDS Turbulent Boundary Layer κ–ε Model Dorodnitsyn Finite Element Heat Transfer

INTRODUCTION

For many flows of practical interest, the viscous effects are confined to regions immediately adjacent to solid surfaces. The finite element method has emerged as a viable alternative to the finite difference method for the solution of laminar and turbulent boundary layer equations. Lynn[4] used a least-squares error criterion to formulate a finite element procedure for the analysis of steady, laminar boundary layer flows. Popinski and Baker[5] used the Galerkin formulation within the method of weighted residuals to cast the two-dimensional boundary layer equations into a standard finite element form. Subsequently, Soliman and Baker[1,6], reported comprehensive numerical results describing accuracy and convergence performance for the finite element algorithm applied to laminar and turbulent boundary layer flow prediction.

The above references have sought, for the two-dimensional incompressible laminar and turbulent boundary layer flows, the velocity components u and v as functions of x and y. In contrast, the Dorodnitsyn finite element algorithm adopted by Fletcher and Fleet[2,3] treats the velocity component u as an independent variable rather than a dependent variable. The Dorodnitsyn formulation is appealing for boundary layer computation since the domain in the y direction is replaced by a fixed finite domain in u. Whereas traditional boundary layer computational schemes require grading with a fine mesh in the near-wall region in order to obtain acceptable results, a uniform grid in u for the Dorodnitsyn formulation automatically provides high resolution (in physical space) close to the wall.

In the present study, we extend the group variable and Dorodnitsyn finite element formulation to treat turbulent boundary layer flow with heat transfer and using a two-equation turbulence model. The resulting coupled system is solved iteratively. Numerical studies are conducted for

0271–2091/86/110769–19$09.50

Received 30 December 1985
Revised 2 April 1986

representative turbulent boundary layer flows. Both algebraic and two-equation turbulence models are considered, and comparison computations are made with finite difference calculations.

GOVERNING EQUATIONS

We consider steady, two-dimensional boundary-layer flows. The time-averaged equation of motion is of the form[7]

$$u\frac{\partial u}{\partial x}+v\frac{\partial u}{\partial y}=u_e\frac{du_e}{dx}+\frac{\partial}{\partial y}\left[(\nu+\nu_T)\frac{\partial u}{\partial y}\right]. \tag{1}$$

In addition, conservation of mass implies

$$\frac{\partial u}{\partial x}+\frac{\partial v}{\partial y}=0. \tag{2}$$

In equations (1) and (2), u and v represent the velocity components in the x and y co-ordinate directions, respectively; u_e is the free-stream velocity, ν is the kinematic viscosity and ν_T is the turbulent eddy diffusivity.

For steady-state heat transfer in the fluid, the thermal energy equation has the following form:

$$u\frac{\partial T}{\partial x}+v\frac{\partial T}{\partial y}=\frac{\partial}{\partial y}\left[(\alpha+\alpha_T)\frac{\partial T}{\partial y}\right], \tag{3}$$

where T is the temperature, α is the thermal diffusivity of the fluid and α_T is the turbulent thermal diffusivity.

The turbulent diffusivities ν_T and α_T are properties of the flow field and not of the fluid. If the flow is laminar, the turbulent flow contributions α_T and ν_T in (3) and (1) are both zero. On the other hand, if the flow is turbulent, the variables u, v and T are time-averaged quantities and are assumed to be independent of time.

MIXING-LENGTH TURBULENCE MODEL

The Prandtl mixing-length theory is one of several schemes which have been used to evaluate the effective turbulent viscosity, ν_T, in the calculation of turbulent boundary layer flows. In this model, the effective viscosity ν_T is expressed as a function of the time-averaged velocity field in the following way:[7]

$$\nu_T=l^2\left|\frac{\partial u}{\partial y}\right|, \tag{4}$$

where l denotes the mixing-length and is a measure of the turbulent length scales in the fluid flow. The following correlation for l, obtained on the basis of experimental data,[8] is the most common form used in boundary layer computations:

$$l=\begin{cases} ky\left[1-\exp\left(-\dfrac{y}{A}\right)\right], & 0<y<\dfrac{\lambda\delta}{k}, \\ \lambda\delta, & y>\dfrac{\lambda\delta}{k}. \end{cases} \tag{5}$$

In equation (5), k is the von Karman constant and δ is the boundary layer thickness (the point where the fluid velocity u is 99 per cent of the free stream velocity u_e). The experimental values of k and λ are 0·41 and 0·085, respectively. The quantity A is an empirically determined effective

sublayer thickness. The empirical correlation described by Kays and Crawford[8] takes into account the effect of pressure gradients and wall transpiration on the sublayer thickness using

$$A = A^+ \nu / \sqrt{(\tau_0/\rho)}, \tag{6}$$

with

$$A^+ = \frac{25{\cdot}0}{a\{v_0^+ + b[P^+/(1+cv_0^+)]\} + 1{\cdot}0}, \tag{7}$$

where

$$P^+ = \frac{\mu \dfrac{\mathrm{d}p}{\mathrm{d}x}}{\rho^{1/2}\tau_0^{3/2}} \tag{8}$$

and

$$v_0^+ = \frac{v_0}{\sqrt{(\tau_0/\rho)}}. \tag{9}$$

In (7) $a = 7{\cdot}1, b = 4{\cdot}25, c = 10{\cdot}0$, for $P^+ \leqslant 0, v_0^+ \geqslant 0$; if $P^+ > 0$, then $b = 2{\cdot}9$ and $c = 0{\cdot}0$; if $v_0^+ < 0$, then $a = 9{\cdot}0$. Here v_0 denotes the velocity of the fluid injected in the normal direction through a porous wall.

TWO-EQUATION MODEL OF TURBULENCE

A popular starting point for higher-order models is the turbulent kinetic energy equation. The form of the two-equation, low-turbulence Reynolds number model used in the present investigation is described by Jones and Launder.[9] The equations describing turbulent kinetic energy κ and dissipation rate ε are, respectively,

$$u\frac{\partial \kappa}{\partial x} + v\frac{\partial \kappa}{\partial y} = \frac{\partial}{\partial y}\left[\left(\nu + \frac{\nu_T}{\sigma_\kappa}\right)\frac{\partial \kappa}{\partial y}\right] + \nu_T\left(\frac{\partial u}{\partial y}\right)^2 - \varepsilon - 2\nu\left(\frac{\partial \kappa^{1/2}}{\partial y}\right)^2 \tag{10}$$

and

$$u\frac{\partial \varepsilon}{\partial x} + v\frac{\partial \varepsilon}{\partial y} = \frac{\partial}{\partial y}\left[\left(\nu + \frac{\nu_T}{\sigma_\varepsilon}\right)\frac{\partial \varepsilon}{\partial y}\right] + C_1\frac{\varepsilon}{\kappa}\nu_T\left(\frac{\partial u}{\partial y}\right)^2 - C_2\frac{\varepsilon^2}{\kappa} + 2\nu\nu_T\left(\frac{\partial^2 u}{\partial y^2}\right)^2. \tag{11}$$

Equations (10) and (11) are based on the assumption that transport by diffusion proceeds at a rate proportional to the product of the turbulent viscosity and the gradient of the property in question (the terms σ_κ and σ_ε thus have the significance of turbulent Prandtl numbers). To complete the specification of the model, the quantities C_1, C_2, σ_κ and σ_ε must be prescribed. The values suggested by Jones and Launder on the basis of experimental data for C_1, σ_κ and σ_ε are 1·45, 1·0 and 1·3, respectively. An empirical correlation is employed to evaluate C_2:

$$C_2 = 2{\cdot}0[1{\cdot}0 - 0{\cdot}3\exp(-R_T^2)]. \tag{12}$$

The constitutive equation relating the turbulent viscosity ν_T to the turbulence kinetic energy and turbulence dissipation rate is

$$\nu_T = C_\mu \frac{\kappa^2}{\varepsilon}, \tag{13}$$

where

$$C_\mu = 0{\cdot}09\exp[-2{\cdot}5/(1 + R_T/50)]. \tag{14}$$

EDDY DIFFUSIVITY FOR HEAT TRANSFER

In order to make heat transfer calculations in turbulent boundary layers, it is necessary to evaluate the eddy diffusivity for heat transfer α_T, so that the thermal energy equation can be solved for the temperature field. The concept of a turbulent Prandtl number for heat transfer, wherein a relationship is sought between α_T and ν_T, is most commonly used in the evaluation of α_T:

$$\alpha_T = \frac{\nu_T}{Pr_T}. \tag{15}$$

An empirical correlation for the turbulent Prandtl number Pr_T, established by Kays and Crawford,[8] has been used in the present investigation:

$$Pr_T = \frac{1}{\dfrac{1}{2Pr_{T\infty}} + C\,Pe_T\sqrt{\left(\dfrac{1}{Pr_{T\infty}}\right) - (C\,Pe_T)^2\left[1 - \exp\left(\dfrac{-1}{C\,Pe_T\sqrt{Pr_{T\infty}}}\right)\right]}}, \tag{16}$$

where

$$Pe_T = \left(\frac{\nu_T}{\nu}\right) Pr. \tag{17}$$

In equation (16), the values 0·2 and 0·86 for C and $Pr_{T\infty}$, respectively, have been observed to yield reasonable correlations. In equation (17), Pr represents the molecular Prandtl number of the fluid. The above correlation appears to fit the available experimental data reasonably well over the practical Prandtl number spectrum.

DORODNITSYN BOUNDARY LAYER FORMULATION

We extend the group variable and Dorodnitsyn finite element approach of Fletcher and Fleet[2,3] to the present two-equation turbulence model with heat transfer. In the Dorodnitsyn formulation, we define

$$\xi = x \quad \text{and} \quad \eta = u_e y \tag{18}$$

and new velocity components

$$u' = u/u_e, \quad v' = v/u_e \quad \text{and} \quad w = v'u_e + \eta\frac{u'}{u_e}\frac{du_e}{d\xi} \tag{19}$$

to transform the governing equations (1), (3), (10) and (11). Using this transformation and, for notational convenience dropping the prime, we may introduce weight functions $f(u'), df(u')/du$ in a weighted average of the momentum and continuity equation, integrate with respect to η and define $\tau = 1/\theta = \partial u/\partial\eta$ to change the variable of integration from η to u, and obtain[3]

$$\frac{\partial}{\partial\xi}\int_0^1 uf\theta\,du - v_0 f(0) = \frac{1}{u_e}\frac{du_e}{d\xi}\int_0^1 (1-u^2)\frac{df}{du}\theta\,du + u_e\int_0^1 \frac{df}{du}\frac{\partial}{\partial u}[(\nu+\nu_T)\tau]\,du. \tag{20}$$

Equation (20) is the Dorodnitsyn formulation for laminar and turbulent boundary layer flows. In equation (20), τ and θ are the dependent variables, and ξ and u are the independent variables. For laminar flows, ν_T is zero, and the effective viscosity is simply the kinematic viscosity ν. For turbulent flows, the effective viscosity is the sum of the laminar component and the turbulent eddy diffusivity ν_T.

For the two-equation model, the governing equations (10) and (11) are transformed to the following equations (after dropping the prime and simplifying):

$$u\frac{\partial \kappa}{\partial \xi}+w\frac{\partial \kappa}{\partial \eta}=u_e\frac{\partial}{\partial \eta}\left[\left(\nu+\frac{\nu_T}{\sigma_\kappa}\right)\frac{\partial \kappa}{\partial \eta}\right]+u_e^3\nu_T\left(\frac{\partial u}{\partial \eta}\right)^2-\frac{\varepsilon}{u_e}-2\nu u_e\left(\frac{\partial \kappa^{1/2}}{\partial \eta}\right)^2, \tag{21}$$

$$u\frac{\partial \varepsilon}{\partial \xi}+w\frac{\partial \varepsilon}{\partial \eta}=u_e\frac{\partial}{\partial \eta}\left[\left(\nu+\frac{\nu_T}{\sigma_\varepsilon}\right)\frac{\partial \varepsilon}{\partial \eta}\right]+C_1u_e^3\frac{\varepsilon}{\kappa}\nu_T\left(\frac{\partial u}{\partial \eta}\right)^2-C_2\frac{1}{u_e}\frac{\varepsilon^2}{\kappa}+2u_e^5\nu\nu_T\left(\frac{\partial^2 u}{\partial \eta^2}\right)^2. \tag{22}$$

Multiplying equations (21) and (22) by the weight function $g(u)$ and integrating across the boundary layer, we have

$$\begin{aligned}\int_0^\infty u\frac{\partial \kappa}{\partial \xi}g\,d\eta+\int_0^\infty w\frac{\partial \kappa}{\partial \eta}g\,d\eta&=u_e\int_0^\infty\frac{\partial}{\partial \eta}\left[\left(\nu+\frac{\nu_T}{\sigma_\kappa}\right)\frac{\partial \kappa}{\partial \eta}\right]g\,d\eta\\&\quad+u_e^3\int_0^\infty\nu_T\left(\frac{\partial u}{\partial \eta}\right)^2g\,d\eta-\frac{1}{u_e}\int_0^\infty\varepsilon g\,d\eta\\&\quad-2\nu u_e\int_0^\infty\left(\frac{\partial \kappa^{1/2}}{\partial \eta}\right)^2g\,d\eta\end{aligned} \tag{23}$$

and

$$\begin{aligned}\int_0^\infty u\frac{\partial \varepsilon}{\partial \xi}g\,d\eta+\int_0^\infty w\frac{\partial \varepsilon}{\partial \eta}g\,d\eta&=u_e\int_0^\infty\frac{\partial}{\partial \eta}\left[\left(\nu+\frac{\nu_T}{\sigma_e}\right)\frac{\partial \varepsilon}{\partial \eta}\right]g\,d\eta\\&\quad+u_e^3\int_0^\infty C_1\frac{\varepsilon}{\kappa}\nu_T\left(\frac{\partial u}{\partial \eta}\right)^2g\,d\eta-\frac{1}{u_e}\int_0^\infty C_2\frac{\varepsilon^2}{\kappa}g\,d\eta\\&\quad+2u_e^5\nu\int_0^\infty\nu_T\left(\frac{\partial^2 u}{\partial \eta^2}\right)^2g\,d\eta.\end{aligned} \tag{24}$$

Upon performing a standard integration by parts with respect to η, on the terms involving second derivatives of κ and ε the following expressions result:

$$u_e\int_0^\infty\frac{\partial}{\partial \eta}\left[\left(\nu+\frac{\nu_T}{\sigma_\kappa}\right)\frac{\partial \kappa}{\partial \eta}\right]g\,d\eta=-u_e\int_0^\infty\left(\nu+\frac{\nu_T}{\sigma_\kappa}\right)\frac{\partial \kappa}{\partial \eta}\frac{\partial g}{\partial \eta}d\eta+\sigma_1(\infty)g(1)-\sigma_1(0)g(0), \tag{25}$$

$$u_e\int_0^\infty\frac{\partial}{\partial \eta}\left[\left(\nu+\frac{\nu_T}{\sigma_\varepsilon}\right)\frac{\partial \varepsilon}{\partial \eta}\right]g\,d\eta=-u_e\int_0^\infty\left(\nu+\frac{\nu_T}{\sigma_\varepsilon}\right)\frac{\partial \varepsilon}{\partial \eta}\frac{\partial g}{\partial \eta}d\eta+\sigma_2(\infty)g(1)-\sigma_2(0)g(0), \tag{26}$$

where

$$\sigma_1(\eta)=\left(\nu+\frac{\nu_T}{\sigma_\kappa}\right)\frac{\partial \kappa}{\partial y}=u_e\left(\nu+\frac{\nu_T}{\sigma_\kappa}\right)\frac{\partial \kappa}{\partial \eta}, \tag{27}$$

$$\sigma_2(\eta)=\left(\nu+\frac{\nu_T}{\sigma_\varepsilon}\right)\frac{\partial \varepsilon}{\partial y}=u_e\left(\nu+\frac{\nu_T}{\sigma_\kappa}\right)\frac{\partial \varepsilon}{\partial \eta}. \tag{28}$$

By introducing equations (25) and (26) into the integral statements (23) and (24), respectively, and changing the variable of integration from η to u,

$$\begin{aligned}\int_0^1 u\frac{\partial \kappa}{\partial \xi}g\theta\,du+\int_0^1 w\frac{\partial \kappa}{\partial u}g\,du&=-u_e\int_0^1\left(\nu+\frac{\nu_T}{\sigma_\kappa}\right)\tau\frac{\partial \kappa}{\partial u}\frac{dg}{du}du\\&\quad+u_e^3\int_0^1\nu_T\tau g\,du-\frac{1}{u_e}\int_0^1\varepsilon g\theta\,du-2\nu u_e\int_0^1\left(\frac{\partial \kappa^{1/2}}{\partial u}\right)^2\tau g\,du\\&\quad+\sigma_1(1)g(1)-\sigma_1(0)g(0)\end{aligned} \tag{29}$$

and

$$\int_0^1 u\frac{\partial \varepsilon}{\partial \xi}g\theta\,\mathrm{d}u + \int_0^1 w\frac{\partial \varepsilon}{\partial u}g\,\mathrm{d}u = -u_e\int_0^1\left(\nu+\frac{\nu_T}{\sigma_\varepsilon}\right)\tau\frac{\partial \varepsilon}{\partial u}\frac{\mathrm{d}g}{\mathrm{d}u}\mathrm{d}u$$
$$+u_e^3\int_0^1 C_1\frac{\varepsilon}{\kappa}\nu_T\tau g\,\mathrm{d}u - \frac{1}{u_e}\int_0^1 C_2\frac{\varepsilon^2}{\kappa}g\theta\,\mathrm{d}u + 2\nu u_e^5\int_0^1 \nu_T\tau\left(\frac{\partial\tau}{\partial u}\right)^2 g\,\mathrm{d}u$$
$$+\sigma_2(1)f(1)-\sigma_2(0)g(0) \tag{30}$$

where

$$\tau = 1/\theta = \frac{\partial u}{\partial \eta} \quad \text{and} \quad w = v'u_e + \eta\frac{u'}{u_e}\frac{\mathrm{d}u_e}{\mathrm{d}\xi}. \tag{31}$$

Equations (29) and (30) represent the Dorodnitsyn formulation for the κ–ε equations: κ and ε are the dependent variables, whereas ξ and u are the independent variables. The free-stream boundary conditions require that $\partial\varepsilon/\partial y$ and $\partial\kappa/\partial y$ be zero at the edge of the layer. Hence, in equations (29) and (30) $\sigma_1(1)=\sigma_2(1)=0$. Furthermore, the boundary terms can be completely eliminated from equations (29) and (30) by choosing a class of weight functions which satisfy the condition $g(0)=0$.

The Dorodnitsyn formulation transforms an infinite y domain to a fixed and finite u domain. This eliminates the need for readjusting the grid in order to accommodate the downstream boundary layer growth. Of greater importance is the fact that a uniform grid in the u direction provides high resolution close to the wall.

FINITE ELEMENT FORMULATION

The computational algorithm is greatly simplified by uncoupling the κ–ε equations from the momentum equation at each step in the ξ direction. The momentum solution $\tau = 1/\theta = \partial u/\partial\eta$ obtained at each ξ location is used in the solution of the parabolic and non-linear κ–ε equations.

Fletcher and Fleet use a group variable formulation wherein a trial expansion is introduced for $(\nu+\nu_T)\tau$ in equation (20). The expansions introduced for θ and $(\nu+\nu_T)\tau$ are

$$\theta = \sum_{j=1}^{M}\theta_j(\xi)\phi_j(u)/(1-u), \tag{32}$$

$$(\nu+\nu_T)\tau = \sum_{j=1}^{M}(\nu+\nu_{T,j})\tau_j(\xi)\phi_j(u)(1-u), \tag{33}$$

where $\phi_j(u)$ are one-dimensional piecewise polynomial finite element basis functions in the transverse (u) co-ordinate direction. The additional factor $(1-u)$ is introduced to ensure that $\theta\to\infty$ and $\tau\to 0$ at the edge of the boundary layer. The group formulation in (33) implies that ν_T need only be evaluated at the grid points. To ensure that w and v do not appear explicitly in equation (20), the condition $f(1)=0$ must be satisfied. Hence, the weight function from the Dorodnitsyn formulation has the following form

$$f(u) = f_i(u) = (1-u)\phi_i(u). \tag{34}$$

Introducing the approximate expansions for θ and τ and the test function above into equation (20) results in a modified Galerkin finite element formulation. Evaluation of the various integrals in equation (20) generates the following semi-discrete system of ordinary differential equations:

$$\sum_j C_{ij}\frac{\mathrm{d}\theta_j}{\mathrm{d}\xi} = \frac{1}{u_e}\frac{\mathrm{d}u_e}{\mathrm{d}\xi}\sum_j A_{ij}\theta_j + u_e\sum_j B_{ij}(\nu+\nu_{T,j})\tau_j, \tag{35}$$

where

$$C_{ij} = \int_0^1 \phi_j \phi_i u \, du, A_{ij} = \int_0^1 \left[\frac{d\phi_i}{du}(1-u) - \phi_i \right] \phi_j (1+u) \, du,$$

$$B_{ij} = \int_0^1 \left[\frac{d\phi_i}{du}(1-u) - \phi_i \right] \left[\frac{d\phi_j}{du}(1-u) - \phi_j \right] du. \tag{36}$$

Note that the dual prescription of both θ and τ prevents the relationship $\theta = 1/\tau$ from being satisfied except at the nodes where $\theta_j = 1/\tau_j$.

Based on the scheme described by Fletcher and Fleet,[3] an implicit algorithm for the marching equation (35) is constructed as follows. Equation (35) is written as

$$\sum_j C_{ij} \Delta\theta_j^{(n+1)} = \Delta\xi \{\omega S^{(n+1)} + (1-\omega) S^{(n)}\}, \tag{37}$$

where

$$S = \frac{1}{u_e} \frac{du_e}{d\xi} \sum_j A_{ij} \theta_j + u_e \sum_j B_{ij} (\nu + \nu_{T,j}) \tau_j + \delta_{1i} v_0 \tag{38}$$

and

$$\delta_{1i} = 1 \quad \text{if} \quad i = 1, 0 \quad \text{if} \quad i \neq 1.$$

Next, $S^{(n+1)}$ is expanded as a function of θ_j, about the known ξ^n level with

$$S^{(n+1)} \approx S^{(n)} + \left[\frac{\partial S}{\partial \theta_j} \right]^{(n)} \Delta\theta_j^{(n+1)}, \tag{39}$$

where

$$\Delta\theta_j^{(n+1)} = \theta_j^{(n+1)} - \theta_j^{(n)}. \tag{40}$$

In the above equations, the superscript n denotes the nth 'time step' in the ξ direction. The resulting implicit system of equations for $\Delta\theta_j^{(n+1)}$ is

$$\sum_j \bar{C}_{ij}^{(n)} \Delta\theta_j^{(n+1)} = P_i, \tag{41}$$

where

$$\bar{C}_{ij} = C_{ij} - \omega \Delta\xi \left[\left(\frac{1}{u_e} \frac{du_e}{d\xi} \right)^{(n+1)} A_{ij} - u_e^{(n+1)} B_{ij} (\nu + \nu_{T,j})^{(n)} \tau_j^{(n)2} \right] \tag{42}$$

$$P_i = \Delta\xi \left\{ \left(\frac{1}{u_e} \frac{du_e}{d\xi} \right)^{(n+1)} \sum_j A_{ij} \theta_j^{(n)} + u_e^{(n+1)} \sum_j B_{ij} (\nu + \nu_{T,j})^{(n)} \tau_j^{(n)} + v_0^{(n+1)} \delta_{1i} \right\}, \tag{43}$$

The parameter ω controls the 'degree of implicitness'—setting $\omega = 0$ gives an explicit marching scheme and $\omega = 1$ a 'fully implicit' method. For the step sizes $\Delta\xi$ used, values of ω below 0·5 and 0·7 for laminar and turbulent flows, respectively, produced unstable numerical results.

The matrix equation (41) is tridiagonal for linear elements and is block diagonal and pentadiagonal for quadratic elements. In the present method, equation (41) is solved for the solution at level $(n+1)$ without iteration within the 'time' step.

The marching algorithm described above uses a variable-step scheme. The step size $\Delta\xi$ is adjusted on the basis of the parameter $\Delta\theta_w^{(n+1)}/\theta_w^{(n)}$. If $\Delta\theta_w^{(n+1)}/\theta_w^{(n)} < (0{\cdot}1)\gamma$, the step size is increased

by 50 per cent (as long as a maximum specified step size is not exceeded. If $\Delta\theta_w^{(n+1)}/\theta_w^{(n)} > \gamma$, the step size is halved (provided a specified minimum step size is exceeded); tolerance γ is specified.

The Dorodnitsyn formulation automatically ensures that the boundary conditions are satisfied, and thus no boundary conditions need be explicitly enforced in the finite element system (41). Furthermore, the matrices in equation (36) may be evaluated 'once and for all', i.e. they need not be evaluated at each step in the ξ direction. When a solution to the thermal energy equation is also desired, the thermal solution is also taken into account in a modified criterion for choosing the step size $\Delta\xi$.

Trial solutions are introduced for κ and ε as

$$\kappa = \sum_{j=1}^{M} \kappa_j(\xi)\phi_j(u)$$

and

$$\varepsilon = \sum_{j=1}^{M} \varepsilon_j(\xi)\phi_j(u), \tag{44}$$

where $\phi_j(u)$ are one-dimensional shape functions in the transverse direction (u). The weight function in equations (29) and (30) has the form

$$g_i(u) = \phi_i(u), \tag{45}$$

where $g_i(u)$ satisfies the condition $g_i(0) = 0$.

Substitution of trial and test functions into equations (29) and (30) generates the following system of ordinary differential equations:

$$\sum_j A_{ij}\frac{d\kappa_j}{d\varepsilon} = -\sum_j [B_{ij} + u_e C_{ij}]\kappa_j + u_e^3 \bar{C}_i - \frac{1}{u_e}\bar{D}_i - 2\nu u_e \bar{E}_i, \tag{46}$$

where

$$A_{ij} = \int_0^1 u\phi_j\phi_i\theta\,du, \quad B_{ij} = \int_0^1 w\frac{d\phi_j}{du}\phi_i\,du,$$

$$C_{ij} = \int_0^1 \left[\nu + \frac{\nu_T}{\sigma_\kappa}\right]\tau\frac{d\phi_i}{du}\frac{d\phi_j}{du}du, \quad \bar{C}_i = \int_0^1 \nu_T\tau\phi_i\,du,$$

$$\bar{D}_i = \int_0^1 \varepsilon\phi_i\theta\,du, \qquad \bar{E}_i = \int_0^1 \left[\frac{\partial\kappa^{1/2}}{\partial u}\right]^2 \tau\phi_i\,du, \tag{47}$$

and

$$\sum_j A_{ij}\frac{d\varepsilon_j}{d\xi} = -\sum_j [B_{ij} + u_e Q_{ij}]\varepsilon_j + u_e^3 \bar{Q}_i - \frac{1}{u_e}\bar{R}_i + 2\nu u_e^5 \bar{S}_i, \tag{48}$$

where

$$Q_{ij} = \int_0^1 \left[\nu + \frac{\nu_T}{\sigma_\varepsilon}\right]\tau\frac{d\phi_j}{du}\frac{d\phi_i}{du}du, \quad \bar{Q}_i = \int_0^1 C_1\frac{\varepsilon}{\kappa}\nu_T\tau\phi_i\,du,$$

$$\bar{R}_i = \int_0^1 C_2\frac{\varepsilon^2}{\kappa}\phi_i\theta\,du, \qquad \bar{S}_i = \int_0^1 \nu_T\tau\left[\frac{\partial\tau}{\partial u}\right]^2\phi_i\,du, \tag{49}$$

Note that in the above expression the approximate expansions for κ and ε are not explicitly indicated in the non-linear terms $\bar{C}_i$, $\bar{D}_i$, $\bar{E}_i$, $\bar{Q}_i$, etc. Rather, an iterative scheme based on the successive approximation method is constructed wherein the non-linear equations for κ and ε are iteratively linearized within each 'time' step in the ξ direction. That is, the non-linear 'source' vectors $\bar{C}_i$, $\bar{D}_i$, $\bar{Q}_i$, etc., in equations (47) and (49) are evaluated at each iteration based on the solutions from the previous iteration. Furthermore, the terms involving ν_T use the turbulent viscosity obtained from the previous iteration.

The marching algorithm for equations (46) and (48) in the ξ direction and also the iterative scheme used to solve the non-linear system of equations are described below.

The systems of ordinary differential equations (46) and (48) are discretized in the (time-like) ξ-direction to obtain.

$$\sum_j A_{ij}^{(n+1)}\left[\frac{\kappa_j^{(n+1,k+1)}-\kappa_j^{(n)}}{\Delta\xi}\right]=-\sum_j[B_{ij}^{(n+1)}+u_e^{(n+1)}C_{ij}^{(n+1,k)}][\omega\kappa_j^{(n+1,k+1)}+(1-\omega)\kappa_j^{(n)}]$$
$$+u_e^{(n+1)^3}\bar{C}_i^{(n+1,k)}-\frac{1}{u_e^{(n+1)}}\bar{D}_i^{(n+1,k)}-2\nu u_e^{(n+1)}\bar{E}_i^{(n+1,k)} \tag{50}$$

and

$$\sum_j A_{ij}^{(n+1)}\left[\frac{\varepsilon_j^{(n+1,k+1)}-\varepsilon_j^{(n)}}{\Delta\xi}\right]=-\sum_j[B_{ij}^{(n+1)}+(u_e^{(n+1)}Q_{ij}^{(n+1,k)}][\omega\varepsilon_j^{(n+1,k+1)}+(1-\omega)\varepsilon_j^{(n)}]$$
$$+u_e^{(n+1)^3}\bar{Q}_i^{(n+1,k)}-\frac{1}{u_e^{(n+1)}}\bar{R}_i^{(n+1,k)}+2\nu u_e^{(n+1)^5}\bar{S}_i^{(n+1,k)}. \tag{51}$$

In the above equations, the index $(n+1)$ denotes the current ξ location and $(k+1)$ denotes the current iteration level at time step $(n+1)$. The momentum equation is uncoupled from the κ–ε equations at each 'time step', and the solution $\tau=1/\theta=\partial u/\partial\eta$ available from the momentum equation at the $(n+1)$th step is used to solve the partial differential equations for κ and ε.

At each step in the ξ direction, the κ and ε equations are solved using an iterative scheme. The non-linearity in the kinetic energy equation arises from the terms $\nu_T(\partial u/\partial y)^2$, ε and $2\nu(\partial\kappa^{1/2}/\partial y)^2$ in the differential equation (10). Furthermore, the diffusion term $\partial/\partial y\{[\nu+(\nu_T/\sigma_\kappa)](\partial\kappa/\partial y)\}$ is also non-linear in nature. The turbulence dissipation rate equation also has similar non-linear terms. The non-linear contributions in equations (50) and (51) at the $(k+1)$th iteration are evaluated on the basis of κ, ε and ν_T calculated at the k^{th} iteration.

The successive approximation scheme involves the evaluation of the terms occurring in equations (50) and (51) and the solution of algebraic systems of equations to obtain the nodal point values $\kappa_j^{(n+1)}$ and $\varepsilon_j^{(n+1)}$ at each iteration. Within each iteration, the κ and ε equations are uncoupled, i.e. the turbulence kinetic energy equation is solved first to obtain $\kappa_j^{(n+1,k+1)}$ which in turn is used in the solution of the turbulence dissipation rate equation so that $\varepsilon_j^{(n+1,k+1)}$ may be obtained. The iterative scheme described above involves the solution of two algebraic systems of equations, for κ_j and ε_j, respectively, at each iteration.

The turbulent viscosity ν_T is computed at the end of each iteration from

$$\nu_{T,j}^{(n+1,k+1)}=\frac{C_\mu\kappa_j^{(n+1,k+1)^2}}{\varepsilon_j^{(n+1,k+1)}}. \tag{52}$$

In the above equation, $v_{T,j}$ represents the turbulent viscosity at node point j. The turbulent viscosity $v_{T,j}$ obtained at the end of each iteration may be under-relaxed to improve stability and covergence using

$$v_{T,j}^{(n+1,k)} = \alpha v_{T,j}^{(n+1,k+1)} + (1-\alpha) v_{T,j}^{(n+1,k)}, \tag{53}$$

where α represents the relaxation factor.

The iterations are performed until the convergence criterion

$$\operatorname*{Max}_j \left| 1 - \frac{v_{T,j}^{(n+1,k)}}{v_{T,j}^{(n+1,k+1)}} \right| \leqq e \tag{54}$$

is satisfied. The tolerance level e used in the present investigation was 10^{-3}.

The Dorodnitsyn formulation for the momentum equation eliminates the normal velocity component, w, from the integral statement. However, w is required in the evaluation of κ and ε and can be determined in a post-processing calculation at the end of each step by integrating the continuity equation (2) across the boundary layer. On transforming the variable of integration from η to u, the resulting equation is

$$w_j = -\frac{\mathrm{d}}{\mathrm{d}\xi} \int_0^{u_j} u\theta \,\mathrm{d}u + v_0, \tag{55}$$

where w_j represents the normal velocity at the grid points and v_0 represents the normal velocity at the wall.

Following a similar procedure to (23)–(29), the Dorodnitsyn formulation for the thermal energy equation becomes

$$\int_0^1 u \frac{\partial T}{\partial \xi} g\theta \,\mathrm{d}u + \int_0^1 w \frac{\partial T}{\partial u} g \,\mathrm{d}u = -u_e \int_0^1 (\alpha + \alpha_T) \tau \frac{\partial T}{\partial u} \frac{\mathrm{d}g}{\mathrm{d}u} \mathrm{d}u - \frac{q(1)}{\rho c_p} g(1) + \frac{q(0)}{\rho c_p} g(0), \tag{56}$$

where q is the flux, ρ is density, c_p is heat capacity,

$$\tau = 1/\theta = \frac{\partial u}{\partial \eta} \quad \text{and} \quad w = v' u_e + \eta \frac{u'}{u_e} \frac{\mathrm{d}u_e}{\mathrm{d}\xi}. \tag{57}$$

The dependent variable in equation (56) is T, whereas ξ and u are independent variables. The free-stream boundary condition at the edge of the thermal boundary layer requires that $\partial T/\partial y$ be zero. Hence, in equation (56), $q(1) = 0$.

A finite element scheme and a marching algorithm can be constructed for equation (56) in a manner similar to that for the κ–ε equations. However, the linearized and uncoupled form of the thermal energy equation within each 'time step' greatly simplifies the computational scheme.

We introduce the finite element expansion for temperature T

$$T = \sum_{j=1}^{M} T_j(\xi) \phi_j(u), \tag{58}$$

where $\phi_j(u)$ are one-dimensional shape functions. The weight function $g(u)$ is again taken to be

$$g_i(u) = \phi_i(u). \tag{59}$$

Substitution of (58) and (59) into the integral statement (56) produces a modified Galerkin finite element formulation. Evaluating the various integrals in equation (56), we generate the following system of ordinary differential equations:

$$\sum_j A_{ij} \frac{\mathrm{d}T_j}{\mathrm{d}\xi} = -\sum_j [B_{ij} + u_e C_{ij}] T_j + \frac{q(0)}{\rho c} \delta_{1i}, \tag{60}$$

where

$$\delta_{1i} = 1 \quad \text{if} \quad i = 1, \quad 0 \quad \text{if} \quad i \neq 1 \tag{61}$$

$$A_{ij} = \int_0^1 u\phi_j\phi_i\theta \mathrm{d}u, \quad B_{ij} = \int_0^1 w\frac{\mathrm{d}\phi_j}{\mathrm{d}u}\phi_i \mathrm{d}u,$$

$$C_{ij} = \int_0^1 (\alpha + \alpha_T)\tau\frac{\mathrm{d}\phi_j}{\mathrm{d}u}\frac{\mathrm{d}\phi_i}{\mathrm{d}u}\mathrm{d}u. \tag{62}$$

A general implicit marching algorithm can be constructed from equation (60):

$$\sum_j A_{ij}^{(n+1)}(\Delta T_j^{(n+1)}/\Delta\xi) = -\sum_j [B_{ij}^{(n+1)} + u_e^{(n+1)}C_{ij}^{(n+1)}][\omega T_j^{(n+1)} + (1-\omega)T_j^{(n)}] + \frac{q_0^{(n+1)}}{\rho c}\delta_{1i}, \tag{63}$$

where the index $(n+1)$ represents the 'time' level $\xi^{(n+1)}$, ω is the parameter controlling the level of implicitness, and

$$\Delta T_j^{(n+1)} = T_j^{(n+1)} - T_j^{(n)}. \tag{64}$$

At each 'time' step, the solution $\tau = 1/\theta = \partial u/\partial\eta$ is obtained from the solution of the momentum equation, and the turbulent viscosity ν_T is computed either from the mixing-length model or from the solution of the κ–ε equations. The turbulent thermal diffusivity α_T is then obtained from equation (15).

Using the computed velocity field, the linear algebraic system of equations (63) can be constructed and solved to yield the temperature, $T_j^{(n+1)}$, at the grid points. If the temperature $T_w(\xi)$ at the wall is specified, this essential boundary condition can be introduced into the algebraic system of equation (63). On the other hand, if the wall heat flux $q_o(\xi)$ is known, it can be specified as a natural boundary condition.

Since the thermal energy equation and momentum equation may require different values of $\Delta\xi$ for stability, a 'time' stepping scheme which depends on both the velocity and temperature fields can be constructed. The criterion applied in the present formulation uses

$$\beta = \mathrm{Max}\left[\frac{\Delta\theta_w^{(n+1)}}{\theta_w^{(n)}}, \frac{\Delta q_w^{(n+1)}}{q_w^{(n)}}\right], \tag{65}$$

where q_w represents the wall heat flux and $\theta_w = \partial u/\partial\eta$ at $\eta = 0$. If $\beta < 0{\cdot}1\gamma$, the step size $\Delta\xi$ is increased by 50 per cent as long as it does not exceed the specified maximum step size. If $\beta > \gamma$, the step size $\Delta\xi$ is halved so long as the minimum step size is exceeded. Numerical experiments indicate that values of the parameter γ equal to 0·02 and 0·10 for turbulent flow and laminar flow computations, respectively, give stable solutions efficiently.

NUMERICAL RESULTS

Mixing-length turbulence model

In this section, the solutions obtained with the Dorodnitsyn finite element formulation are compared with those obtained using a representative finite difference program STAN5[10] for the case of flow over a flat plate, both with and without blowing in the normal direction. Both computational schemes employed a mixing-length model to calculate the turbulent eddy viscosity.

The wall temperature T_0, free stream temperature T_e and normal velocity at the wall v_0 were held constant in the downstream direction. Results were obtained for values of the blowing fraction $F = (v_0/u_e)$ equal to $+0{\cdot}002$, 0, and $-0{\cdot}002$; $F = -0{\cdot}002$ corresponds to the suction through the wall, whereas $F = 0{\cdot}002$ corresponds to normal wall blowing.

From a practical viewpoint, the skin friction coefficient C_f, the shape factor H and Stanton number St are of interest. These parameters are defined as follows:

$$C_f = \nu \frac{\partial u}{\partial y}\bigg|_{y=0} \Big/ (\tfrac{1}{2}u_e^2), \tag{66}$$

$$St = -\alpha \frac{\partial T}{\partial y}\bigg|_{y=0} \Big/ [u_e(T_0 - T_e)] \tag{67}$$

$$H = \int_0^\infty \left(1 - \frac{u}{u_e}\right) dy \Big/ \left[\int_0^\infty \frac{u}{u_e}\left(1 - \frac{u}{u_e}\right) dy\right]. \tag{68}$$

Graphs of C_f, H and St with downstream position are shown in Figures 1–3. In each case, a uniform grid of 21 linear elements was used. The step size control parameter, γ, and the degree of implicitness, ω, were set at 0·02 and 0·70, respectively, as indicated earlier. It can be observed that the finite element results and those obtained using STAN5 show excellent agreement for all three blowing fractions. From Figures 1 and 3, it can be observed that blowing reduces the skin friction and Stanton number, whereas suction has the reverse effect. Experimental observations[8] indicate that wall blowing destabilizes the flow and promotes boundary layer separation, whereas suction inhibits boundary layer separation, and this is consistent with our numerical results.

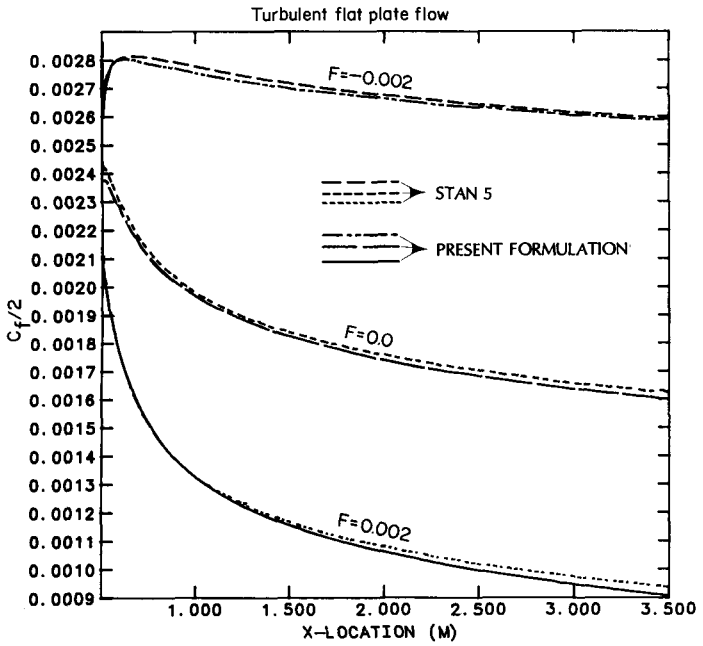

Figure 1. Skin friction for different blowing fractions, F

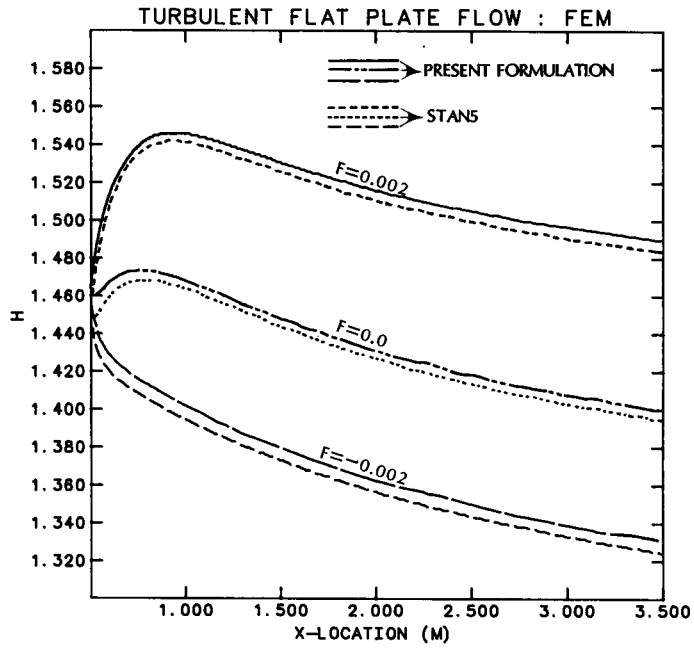

Figure 2. Shape factor for different blowing fractions, F

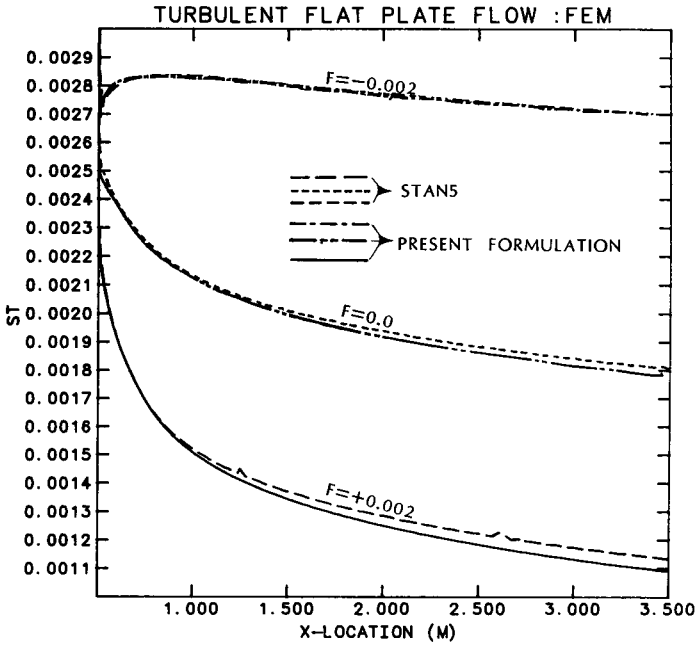

Figure 3. Stanton number for different blowing fractions, F

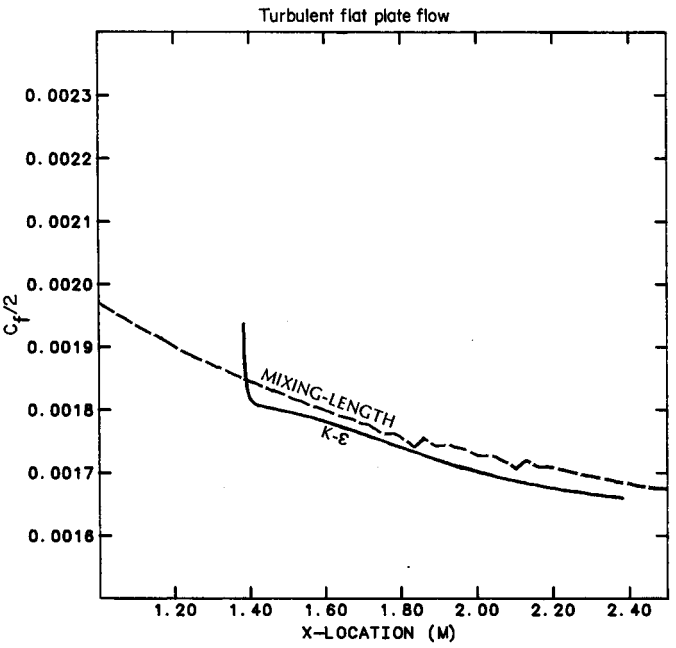

Figure 4. Skin friction as a function of X-location

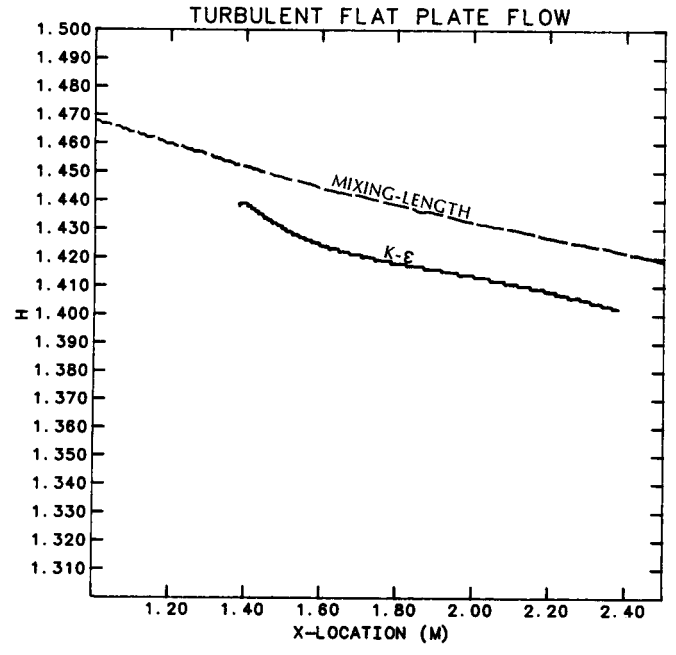

Figure 5. Shape factor as a function of X-location

Two-equation turbulence model

Solutions to the momentum boundary layer equation were obtained using the κ–ε model for the basic case of zero pressure gradient flow. The initial profiles for the turbulent kinetic energy κ and dissipation rate ε were constructed from the algebraic mixing-length scheme based on the procedure described by Soliman and Baker.[1] Figures 4 and 5 represent the variation in skin friction and shape factor with downstream position. It can be observed from Figures 4 and 5 that the mixing-length model and the two-equation model agree closely with each other. Although the initial profiles specified for κ and ε predict the shape factor H accurately, the skin friction C_f predicted in the far upstream section of the flow does not agree closely with that predicted by the mixing-length solution. This probably results from the inaccuracy involved in the initial profiles specified for κ and ε in the near-wall region. However, the two-equation model predicts the correct behaviour in C_f after a few downstream steps.

The velocity profile across the boundary layer at a particular x location ($x = 2{\cdot}5$ m) is given in Figure 6. Also indicated here for qualitative comparison are the results obtained from the mixing-length model and the semi-empirical law-of-wall profile. The velocity profile obtained from the two-equation model exhibits excellent agreement with that obtained from the mixing-length model, verifying the model and implementation for standard flow problems.

The Dorodnitsyn finite element scheme employing the κ–ε model requires a uniform grid of 30 linear elements across the layer to generate adequate solutions. The behaviour of κ across the boundary layer is graphed in Figure 7. Clearly, the solution to the turbulent kinetic energy equation in (x,y) co-ordinates would require a highly graded mesh with a large number of grid points in the near-wall region to capture suitably the rapid changes in κ in this region. However, the turbulent kinetic energy profile in the transformed u-co-ordinate (Figure 8) exhibits a far smoother behaviour. This results in accurate solutions on coarse and uniform grids when the

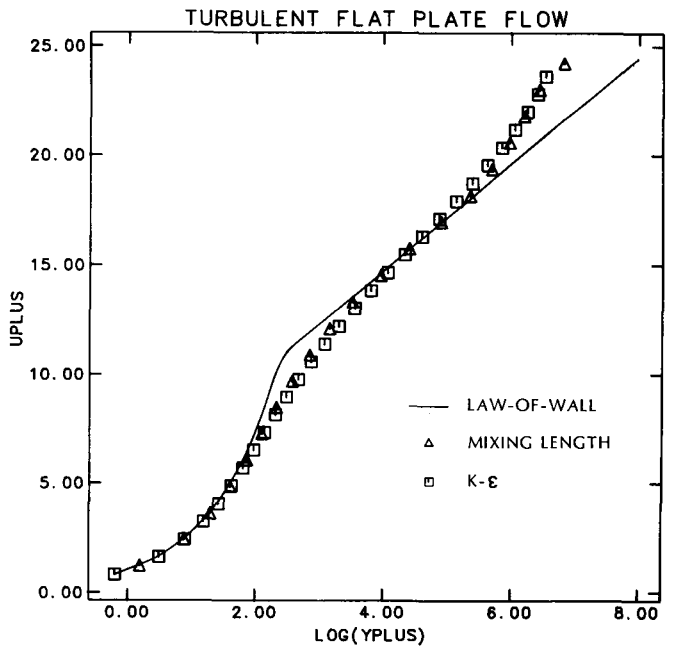

Figure 6. Comparison of velocity profiles across layer

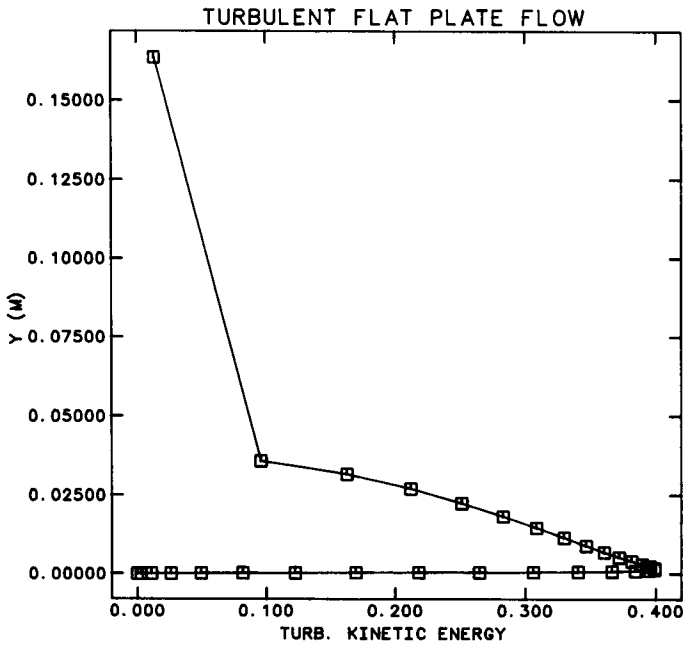

Figure 7. Turbulent kinetic energy κ across layer for 'physical' Y-co-ordinates

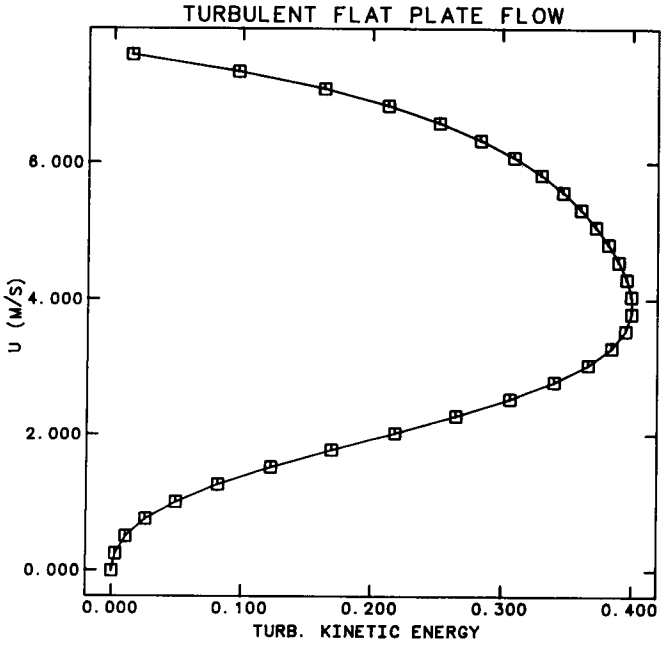

Figure 8. Turbulent kinetic energy across layer for transformed U-co-ordinate

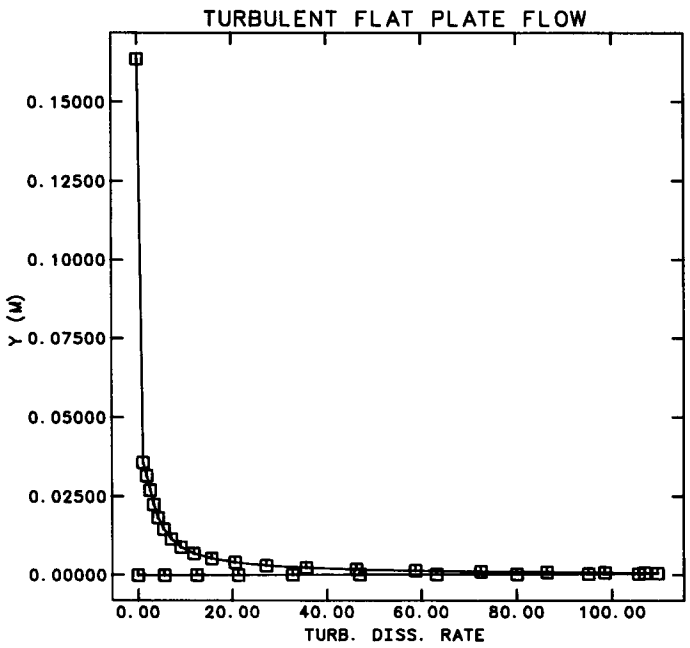

Figure 9. Turbulent dissipation rate ε across layer for 'physical' Y-co-ordinates

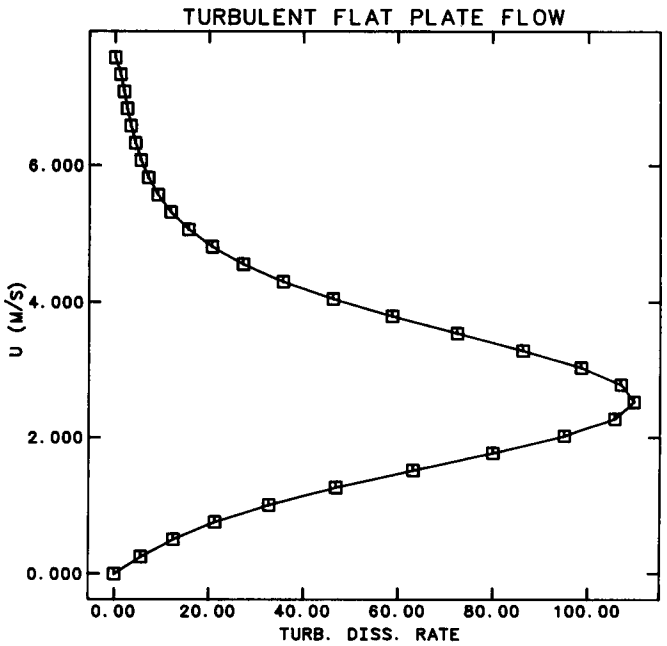

Figure 10. Turbulent dissipation rate across layer for transformed U-co-ordinate

Dorodnitsyn finite element formulation is used. The turbulence dissipation rate ε also exhibits a similar trend across the boundary layer (Figures 9 and 10).

The Dorodnitsyn formulation employing the two-equation model required extremely small downstream steps Δx to generate stable solutions. This is due to the non-linearity and strong coupling between the κ and ε equations. Here, the downstream step sizes ranged from $0{\cdot}6 \times 10^{-4}$ m to $0{\cdot}15 \times 10^{-2}$ m for the two-equation model which can be compared with step sizes ranging from $0{\cdot}4 \times 10^{-3}$ m to 0·14 m for the algebraic mixing-length model. This is a severe practical limitation to design analysis based on the two-equation model.

CONCLUDING REMARKS

In this study, the problem of approximate analysis of laminar and turbulent boundary layer flows is considered. A formal development of the Dorodnitsyn formulation using finite elements and its extension to the two-equation model of turbulence has been given. The non-linear nature of the κ–ε equations in the two-equation model induces severe restrictions on the downstream step sizes in numerical solutions, which impose practical limitations on the scheme. However, a detailed description of the behaviour of turbulence kinetic energy and dissipation rate provide a greater insight into the phenomenon.

The capability of the Dorodnitsyn formulation to capture gradients in the boundary layer leads to a computationally efficient finite element algorithm. The Dorodnitsyn scheme provides accurate results even on coarse grids and does not require graded meshes such as those needed by more standard numerical schemes.[11]

NOMENCLATURE

a	constant in the mixing-length model
A	effective sublayer thickness in the mixing-length model
b, c	constants in the mixing-length model
C_1, C_2, C_μ	constants in the two-equation model
C_f	skin friction coefficient
f	weight function
F	wall blowing fraction
g	weight function
H	shape factor
k	von Karman constant in the mixing-length model
l	Prandtl's mixing length
Pr	molecular Prandtl number
Pr_T	turbulent Prandtl number for heat transfer
R_T	Reynolds number of turbulence
St	Stanton number
T	temperature
u, v	velocity components
v_0	velocity of the fluid injected through the wall

Greek symbols

α	thermal diffusivity
α_T	turbulent thermal diffusivity
γ	step size control parameter

Δ	increment
δ	boundary layer thickness
ε	rate of dissipation of turbulence energy
κ	turbulent kinetic energy
λ	constant in the mixing-length model
ν	kinematic viscosity
ν_T	turbulent viscosity
ρ	density
$\sigma_\kappa, \sigma_\varepsilon$	turbulent Prandtl numbers
τ_0	wall shear stress
ω	degree of implicitness

Subscripts

e	quantity evaluated at the free stream
$0, w$	quantity evaluated at the wall

Superscripts

k	iteration level
n	time step level
$+$	quantity non-dimensionalized by means of μ, τ_0 and ρ

REFERENCES

1. M. O. Soliman and A. J. Baker, 'Accuracy and convergence of a finite element algorithm for turbulent boundary layer flow', *Comp. Meth. Appl. Mech. Eng.* **28**, 81–102 (1981).
2. C. A. J. Fletcher and R. W. Fleet, 'A Dorodnitsyn finite element formulation for laminar boundary layer flow', *Int. j. numer. methods fluids*, **4**, 399–419 (1984).
3. C. A. J. Fletcher and R. W. Fleet, 'A Dorodnitsyn finite element formulation for turbulent boundary layers', *J. Computers and Fluids*, **12** (1), 31–45 (1984).
4. P. O. Lynn, 'Least squares finite element analysis of laminar boundary layers', *Int. j. numer. methods eng.* **8**, 865–876 (1974).
5. Z. Popinski and A. J. Baker, 'An implicit finite element algorithm for the boundary layer equations', *J. Comp. Phys.*, **21**, (1), 55–84 (1976).
6. M. O. Soliman and A. J. Baker, 'Accuracy and convergence of a finite element algorithm for laminar boundary layer flow', *J. Computers and Fluids*, **9**, 43–62 (1981).
7. H. Schlicting, Boundary Layer Theory, 6th eds, McGraw-Hill, 1968.
8. W. M. Kays and M. E. Crawford, *Convective Heat and Mass Transfer*, McGraw-Hill, 1980.
9. W. P. Jones and B. E. Launder, 'The calculation of low-Reynolds-number phenomena with a two-equation model of turbulence', *Int. J. Heat Mass Transfer* **16**, 119–1130 (1973).
10. M. E. Crawford and W. M. K. Kays, 'STAN5—a program for numerical computation of two-dimensional internal and external boundary layer flows', *NASA CR-2742*, 1976.
11. E. B. Becker, G. F. Carey and J. T. Oden, *Finite Elements—An Introduction, Vol. 1*, Prentice-Hall, 1981.